

Flight Control Design and Demonstration of Unmanned Airplane for Radiation Monitoring System

Masayuki Sato* Koji Muraoka* Koki Hozumi*

* Japan Aerospace Exploration Agency, Mitaka, Tokyo 181-0015 Japan
(e-mail: {sato.masayuki, muraoka.koji, hozumi.koki}@jaxa.jp)

Abstract: Fukushima Dai-ichi nuclear power plant received a severe damage due to huge tsunami waves caused by the Great East Japan Earthquake in 2011. This tragedy requires radiation monitoring around the plant using unmanned systems, this paper therefore addresses the flight controller design for an unmanned airplane which is developed for the radiation monitoring. The flight controller has a conventional structure, i.e. Stability/Control Augmentation System (S/CAS) and guidance loops using PID controllers. The controller gains are determined by minimizing appropriately defined cost functions for several models; that is, the worst control performance among multiple models is minimized to obtain robust flight controller gains (so-called “multiple model approach”). Control performance of our flight controller was evaluated through flight tests and preliminary demonstration flights were conducted near the plant.

1. INTRODUCTION

Unmanned Aerial Vehicles (UAVs) and Unmanned Aerial Systems (UASs) have been gaining much attention as tools for practical applications such as surveillance, monitoring and scientific measurement in outdoor environments. Technical reports on this topic have recently been published, e.g. [Cox et al., 2004, DoD, 2005]. This situation encourages engineers and researchers towards the development of UAVs and UASs. (See [DoD, 2005, Valavanis, 2007, Daly, 2011, Valavanis, 2012] for further information.) Some UAVs and UASs are currently in use in real missions, in particular, in military missions.

The Great East Japan Earthquake in 2011 caused severe damages to Japan. In particular, Fukushima Dai-ichi nuclear power plant received severe damages, which resulted in radiological contamination spread [IAE, 2011]. This disaster requires radiation monitoring systems to examine radiological dosage around the power plant. To this end, manned helicopters [MEX, 2011] and unmanned small helicopters [Sato and Imai, 2011], which had been developed before the accident [Okuyama et al., 2008], have been used. However, they have complementary advantages and disadvantages: Manned helicopters are expensive and require a lot of administrative procedures for their execution but the monitoring area is very large. On the other hand, unmanned helicopters are less expensive and can be operated easily but the monitoring area is not so large. One of the solutions to compensate for these disadvantages is to use unmanned airplanes. Japan Aerospace Exploration Agency (JAXA) and Japan Atomic Energy Agency (JAEA) have therefore been developing an airplane together as a radiation monitoring system.

This paper shows the design of the flight controller for the unmanned airplane named as “Unmanned Airplane for Radiation Monitoring System”, in short, UARMS. (The photograph of UARMS is shown in Fig. 1, and the



Fig. 1. UARMS (The blue box under the fuselage is a part of radiation measurement apparatus.)

vehicle’s dimensions are given in Table 1.) Due to the limited onboard computing power, the flight controller has a conventional structure; that is, Stability/Control Augmentation Systems (S/CAS) are applied to enhance the stability and to embed servomechanism for pitch/roll control, and guidance loops composed of Proportional-Integral-Derivative (PID) controllers are applied to control speed, track angle, and the vehicle’s position in three-dimensional space.

Those controllers are required to be robust against modeling errors, such as estimation errors of aerodynamic characteristics, and to be also robust against operating condition change, such as weight changes due to long flight, etc. To this end, *multiple model approach*, which has been originally proposed in [Ackermann, 1985], is adopted in this paper. This is because the usefulness and the effectiveness of the *multiple model approach* for the *a priori* structurally defined controllers have been confirmed in the literature, e.g. [Miyazawa, 1992, Sato and Muraoka, 2013],

Table 1. Dimensions of UARMS

Length	2700 [mm]
Span	4200 [mm]
Height	1315 [mm]
Cruise speed	30 [m/s]
Max. take-off weight	50.0 [kg]
Max. flight hour	6.0 [hr]
Engine	Desert Aircraft DA-100L
Fuel	gasoline
Propellers	26 [inch] \times 12 [pitch] (2 blades)
Sensors	GPS/INS, radio control gyros, air data sensor

etc. The basic multiple models in the method are chosen as linearized aircraft motion models at extreme flight conditions, i.e. four flight conditions at maximum/minimum supposed weight and airspeed. Several additional models are also incorporated with the basic models to enhance robustness of the controllers.

The control performance of our flight controller was examined through flight tests after nonlinear simulation check with wind turbulence given by the Dryden model. Demonstration flights were also conducted near the plant. The demonstration flight results are included in the paper.

This paper is organized as follows: Section 2 describes the flight controller of UARMS and the design results; section 3 shows the results of the demonstration flight; and finally section 4 gives concluding remarks.

The nomenclature related to aircraft motions is fairly standard, but it is summarized below. u, v, w denote the x -, y -, and z -component deviation airspeed of the vehicle from the initial values, p, q, r denote the vehicle's attitude rates, ϕ, θ denote the vehicle's attitude deviations from the initial values, ϕ_{com}, θ_{com} denote their commands, Φ, Θ denote the sums of ϕ, θ and their initial values, Ψ_{trk} denotes track angle, Ψ_{trkcom} denotes its command, $\delta_{elv}, \delta_{ail}, \delta_{rud}$ denote elevator, aileron and rudder deflections, $\delta_{elvc}, \delta_{ailc}, \delta_{rudc}$ denote their commands, δ_{th} and δ_{thc} respectively denote throttle deviation and its command, T_a and T_{th} respectively denote the time constants of modeled actuators and engine dynamics, V and V_{com} respectively denote airspeed and its command, H and H_{com} respectively denote pressure altitude and its command, and Y_{pos} and Y_{com} respectively denote the vehicle's deviation from track course and its command, i.e. 0.

2. FLIGHT CONTROLLER OF UARMS

We first show control requirements and the control structure to satisfy them, then show our adopted design method, i.e. *multiple model approach*, and finally show some details for designing the controller gains of UARMS.

2.1 Control Requirements

The objective of developing UARMS is precise radiation monitoring in wide area. To this end, UARMS is required to satisfy the following requirements:

- Precise vehicle's position control in three dimensional space, in particular, precise path-following for *a priori* designated straight courses irrespective of wind turbulences

The maximum errors of altitude and horizontal path following are both recommended within 5 [m]. The radiation monitoring is presumed to be conducted on straight courses, the latter requirement is thus imposed. Realizing the above requirements possibly leads to terrain-following techniques as in [Williams, 2007].

In addition to the above requirements, airspeed control is required to prevent stall and overload due to overspeed.

2.2 Flight Control Structure

Considering that the prevailing flight control structure has been suitably developed for controlling airplane motions, a similar structure is adopted for UARMS. The block diagrams for the longitudinal and lateral-directional motions of UARMS are respectively shown in Figs. 2 and 3. There are many hidden components, such as integral calculation limits, command limits, etc., to prevent unrealistic commands, and logical components, such as automatic leg change calculation components, etc., they are all omitted for brevity. The basic structure is PID controller, though some explanations for the structure are given below.

The SAS which feeds back attitude rate signals p, q is very common to enhance the stability of vehicle's rotational motions, and CAS which feeds back the error between attitude signals θ, ϕ and their commands is also common to implement servomechanism for attitude control. A feedback loop from attitude rate signal r to rudder is very useful to enhance the stability of the lateral-directional motions; however, the rudder is set to be used only as an emergency input to make UARMS fall down within the designated area. Speed control and altitude control in longitudinal motions are composed of simple PID controllers. The cross term from the altitude error to throttle is applied because altitude changes usually require energy adjustment, i.e. throttle changes. On the other hand, the converse, i.e. the cross term from speed error to altitude change, is not applied, because precise speed control is not required for UARMS. In the lateral-directional motions, the track angle control is composed only of a proportional controller but with its gain depending on the track angle error. The error-dependent gain produces appropriately large roll command even when the error is small while oscillatory roll motions due to excessively large gains can be prevented. This leads to "precise horizontal path-following control" without closed-loop instability. Furthermore, the error between the designated course angle and vehicle's track angle is used for generating the track angle command to counteract wind turbulence very quickly.

2.3 Framework of Robust Controller Gain Design via Multiple Model Approach

We briefly review the concept of *multiple model approach* in [Ackermann, 1985] and show some extensions below.

Let us consider the case in which the structure of the controller is defined *a priori* and only controller gains are to be designed to satisfy robust control requirements. Suppose that multiple models which represent possible uncertainty effects and possible operating conditions are given. Then, the design problem of the controller gains can be defined as follows [Ackermann, 1985]:

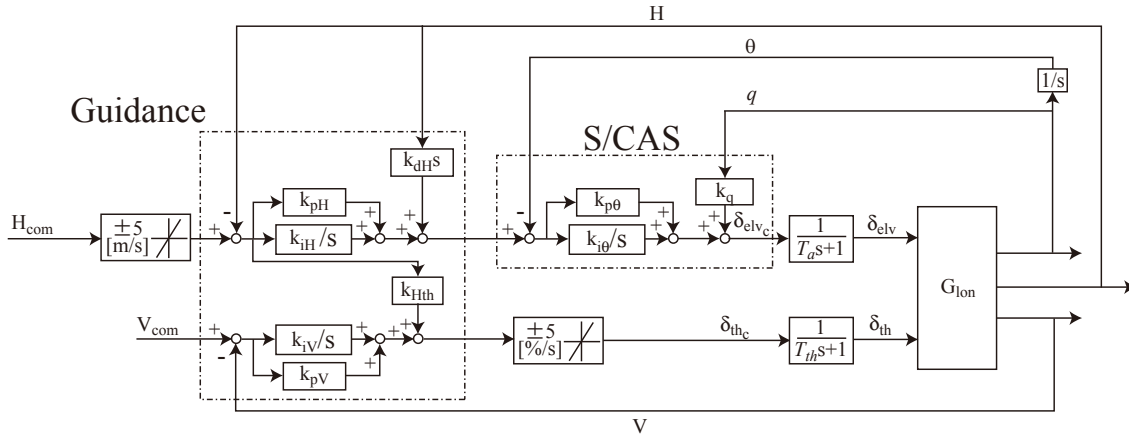


Fig. 2. Block diagram of guidance and control for longitudinal motions

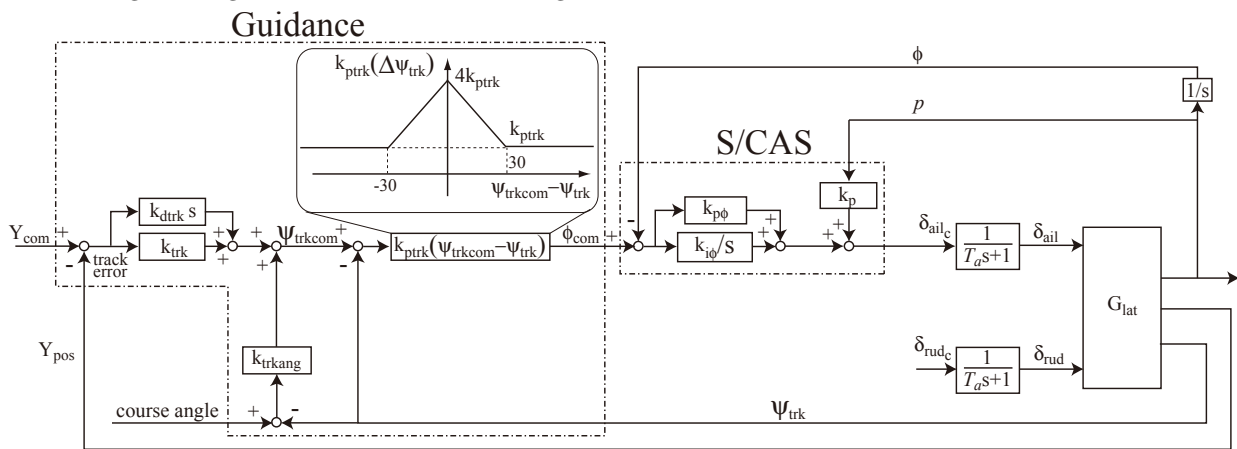


Fig. 3. Block diagram of guidance and control for lateral-directional motions

$$\min_k \max_{\text{multiple models}} f_{\text{cost}}(k) \quad (1)$$

where vector k denotes a vector of gains to be designed, and $f_{\text{cost}}(k)$ denotes an appropriately defined cost function representing control requirements.

This formulation is simple and reasonable because the worst cost among supposed models to be considered is minimized by choosing controller gain vector k appropriately. However, if the admissible region of the gains is not set or the multiple models are not suitably set, then formulation (1) often produces unrealistically large gains. Furthermore, some constraints of controlled plant outputs are usually imposed to prevent over-shoot, or to minimize settling time, etc. We thus revise the formulation (1) to prevent unrealistic large gains and to satisfy the constraints of the plant outputs as follows:

$$\min_{k \in \mathcal{K}} \max_{\text{multiple models}} f_{\text{cost}}(k) \text{ s.t. } g_i \leq 0 \quad (i = 1, \dots, m) \quad (2)$$

where \mathcal{K} denotes the *a priori* defined admissible gain set, and $g_i \leq 0 \quad (i = 1, \dots, m)$ denote the constraints to be satisfied. This formulation can be simplified as follows with very large constant weights $\lambda_i \quad (i = 1, \dots, m)$:

$$\min_{k \in \mathcal{K}} \max_{\text{multiple models}} f_{\text{cost}}(k) + \sum_{i=1}^m \lambda_i g_i \quad (3)$$

The set \mathcal{K} can be defined by numerical simulations, or by considering the characteristics of the plant dynamics.

When possible disturbances to the plant can be estimated *a priori*, and robust control performance against uncertainties, various operating conditions, and possible disturbances is to be minimized, the formulation (3) should be further revised. We propose the following formulation:

$$\min_{k \in \mathcal{K}} \max_{d \in \mathcal{D}} \max_{\text{multiple models}} f_{\text{cost}}(k, d) + \sum_{i=1}^m \lambda_i g_i \quad (4)$$

where d and \mathcal{D} respectively denote the disturbance and the *a priori* defined finitely many possible disturbance set.

The approach above does not guarantee robust performance for all possible *infinitely many* models like H_∞ control, but only guarantees it for all supposed *finitely many* models. This is one of the disadvantages of the method; however the formulation can produce *a priori* structurally defined controller gains with its robust performance being optimized, which is one of the advantages of the method. Considering that the flight controller structure of UARMS is defined in advance, the above method is adopted.

2.4 Design Problem Setup for UARMS

The design of the flight controller gains was conducted step by step; that is, the S/CAS gains are first designed, then

the guidance loop gains are designed. In the longitudinal guidance loop gain design, the speed hold loop gains are first designed, then the altitude hold loop gains are designed, and the cross term gain is finally designed. This is because, under an ideal condition, altitude is given as $\int V \sin(\Theta - \alpha) dt$, where α denotes angle of attack, so altitude control performance heavily depends on speed and attitude control performances. Thus, speed control design is conducted prior to altitude control design.

UARMS is nominally presumed to fly with its airspeed of 30 [m/s]; however, wind gust inevitably exists in outdoor environments. Thus, two models at 25 [m/s] and 35 [m/s] are considered. The weight is supposed to deviate from 50 [kg] to 40 [kg] during flight. We therefore use four linearized aircraft motion models at 40 or 50 [kg] weight, and at 25 or 35 [m/s] airspeed. The engine dynamics from the rotational command to the actual rotation are modeled as a serially connected system of a first-order model $\frac{1}{0.23s+1}$ and a dead time system. It is very hard to estimate the dead time precisely; however, it is not so hard to estimate the range of possible dead time. The dead time range was estimated as [0.1, 0.3] [s]. Thus, in guidance loop gain design, two engine models with dead time of 0.1 [s] and 0.3 [s] are used in addition to the above four models; that is, eight models are used as “multiple models” in the longitudinal guidance loop gain design.

The state variables in the longitudinal and lateral-directional motions are respectively set as $[u \ w \ q \ \theta]^T$ and $[v \ p \ \phi \ r]^T$. In the longitudinal motions, airspeed V is calculated as $\sqrt{(U_0 + u)^2 + (W_0 + w)^2}$ and altitude H is calculated as $\int V \sin(\Theta_0 + \theta - \arctan \frac{W_0 + w}{U_0 + u}) dt$ using the initial forward speed U_0 [m/s], the initial vertical speed W_0 [m/s], and the initial pitch angle Θ_0 . In the lateral-directional motions, track angle Ψ_{trk} in track angle hold loop gain design is calculated as $\int \frac{r}{\cos \Theta_0} dt$.

In the design of S/CAS gains and guidance loop gains apart from track course hold loop gain design, formulation (3) is used since the effect of disturbance, i.e. wind gust, is not so severe. In contrast, in track course hold loop gain design, formulation (4) is used to consider disturbance effect, because wind gust strongly effects the control performance. Thus, in track course hold loop gain design, the vehicle’s x - and y -positions are respectively calculated as $\int V_{I_x} dt$ and $\int V_{I_y} dt$ with x -component inertial speed V_{I_x} and y -component inertial speed V_{I_y} . The speed V_{I_x} is calculated as $V \cos \Psi + U_g$ using yaw angle Ψ and x -component gust U_g . The speed V_{I_y} is calculated by using the lateral-directional motion equations with y -component gust V_g being incorporated. The track angle Ψ_{trk} is correspondingly revised.

In all controller gain design, the cost function $f_{cost}(k)$ in our design is set as follows:

$$f_{cost}(k) = \int_0^{T_{eval}} (x - x_{com})^2 dt, \quad (5)$$

where x and x_{com} respectively denote the performance output and its command, and T_{eval} is evaluation time which is set *a priori*.

Table 2. Performance outputs and commands

	x	x_{com}
S/CAS for lon. motions	θ	unit step command
S/CAS for lat. motions	ϕ	unit step command
Speed hold loop	V	+5 [m/s] step command from the initial speed
Altitude hold loop	H	+10 [m] step command from the initial altitude
Cross term	V	zero deviations from the initial speed for ± 20 [m] altitude change command
Track angle hold loop	Ψ_{trk}	45 [deg] step command
Track course hold loop	Y_{pos}	300 [m] step command

Table 3. Overshoot constraints

	desired constraint	strict constraint
S/CAS for lon. motions	$\theta \leq 1.1$	$\theta \leq 1.25$
S/CAS for lat. motions	$\phi \leq 1.0$	$\phi \leq 1.1$
Speed hold loop	$V \leq 5.0$	$V \leq 5.5$
Altitude hold loop	$H \leq 10.5$	$H \leq 11$
Cross term	$ V \leq 3$	$ V \leq 6$
Track angle hold loop	$\Psi_{trk} \leq 45$	$\Psi_{trk} \leq 46$
Track position hold loop	$Y_{pos} \leq 300$	$Y_{pos} \leq 305$

Table 4. Settling time and evaluation time

	5% settling time [s]	0.1% settling time [s]	T_{eval} [s]
S/CAS for lon. motions	10	20	40
S/CAS for lat. motions	2	4	20
Speed hold loop	10	20	50
Altitude hold loop	20	30	50
Cross term	–	–	100
Track angle hold loop	10	15	30
Track position hold loop	40	80	100

The supposed maximum steady wind of UARMS operation is 15 [m/s] on the ground. Thus, in the design of track course hold loop gains, four scenarios in which steady winds with 20 [m/s] blow from right- or left-hand side, and from the front or backward side are considered.

The performance output in (5) and its command are set as in Table 2.

Regarding the constraints g_i in (3) and (4), two types of constraints are used; one is “desired constraints” which is desired to be satisfied, and the other is “strict constraints” which should be satisfied rigorously. The constant weights for the latter is set as 1000 times larger than the former.

The overshoot constraints for the vehicle’s motions are given in Table 3. The settling time constraints and the evaluation time T_{eval} are given in Table 4. Settling time constraints are all set as “desired constraints”, because the most important control requirement for UARMS is precise position control, e.g. in space domain, not in time domain.

The admissible region \mathcal{K} is set after several trial-and-errors with numerical simulations by using linearized motion equations of UARMS.

The cost function in (3) and (4) were calculated by using MATLAB[®] Simulink, and the optimization was conducted using the MATLAB[®] command “lsqnonlin”.

One example of our design results is shown in Fig. 4 in which the optimized responses of altitude changes and

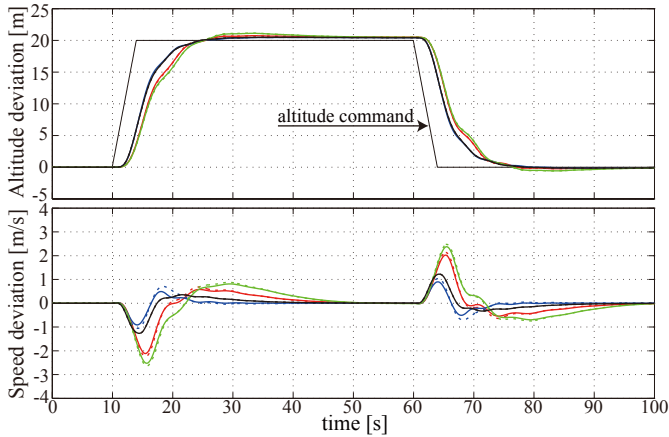


Fig. 4. Cross term design result for ± 20 [m] altitude changes with optimal cross term k_{Hth}

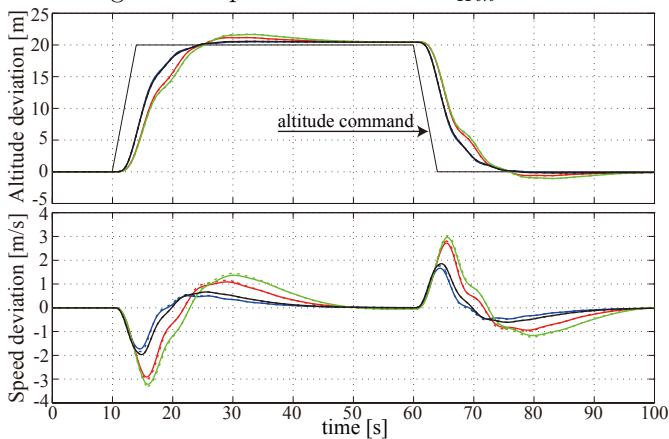


Fig. 5. Cross term design result for ± 20 [m] altitude changes with cross term k_{Hth} being set 0

accompanying speed deviations are shown in the design of cross term gain. For comparison, the counterpart results with the cross term k_{Hth} being set 0 are shown in Fig. 5. In these figures, solid lines and broken lines respectively denote the responses for minimum engine delay (0.1 [s]) and maximum engine delay (0.3 [s]). Similarly, red lines, blue lines, green lines and black lines respectively denote the responses of models with weight of 40 [kg] and airspeed of 25 [m/s], with weight of 40 [kg] and airspeed of 35 [m/s], with weight of 50 [kg] and airspeed of 25 [m/s], and with weight of 50 [kg] and airspeed of 35 [m/s]. It is confirmed that the designed cross term gain certainly reduces the speed deviations as well as the error between altitude and its command when altitude commands change.

After the design of all controller gains, nonlinear simulations were conducted to evaluate control performance using nonlinear equations with aerodynamic coefficient tables. The simulation results showed that satisfactory control performance was expected in real environments

3. FLIGHT TESTS

The control performance of our flight controller was examined through flight tests conducted in a flight test area in Hokkaido (northern Japan). It was confirmed that the designed flight controller has extremely satisfactory performance in calm conditions and satisfactory performance in



Fig. 6. Horizontal view of path-following for radiation monitoring demonstration (“x” and “o” respectively denote the autopilot engage and disengage points.)

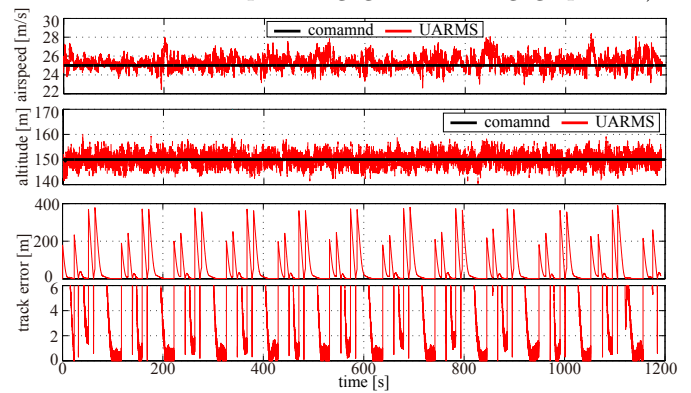


Fig. 7. Time history of airspeed, altitude, and track errors (The fourth row is a close-look of the third row.)

windy conditions. Then, preliminary demonstration flights were conducted in Namie town near the Fukushima Dai-ichi nuclear power plant. Flight results are given below.

Figs. 6 shows the horizontal view of the flight trajectory of a demonstration flight. The flight was conducted under about 8 [m/s] steady wind from the south, which led to some deviations from the designated course. The time history of airspeed, altitude, and track errors are shown in Fig. 7. The airspeed command was given as 25 [m/s], because the air data sensor gives biased values with about 5 [m/s] below from the actual data. The altitude command was given as a constant value of 150 [m] in pressure altitude. It is confirmed that altitude error was almost within 5 [m], airspeed error was almost within 2 [m/s], and track course error on straight lines after crossing the lines was almost within 2 [m] in windy real environments.

Figs. 8 shows the vertical view of the flight trajectory of another demonstration flight with several altitude command changes. Steady wind blew with about 4 [m/s] up to 8 [m/s]. The time histories of altitude and its error are shown in Fig. 9. It is confirmed that large discrepancies exist just after altitude changes are applied. This is mainly because the engine rotation could not be reduced due to the minimum throttle setting for safety. Thus, a revision for throttle setting for safety will be revised for control performance improvement.

ACKNOWLEDGEMENTS

The authors are grateful for the very kind support of the municipalities for the preliminary demonstration flights as well as JAEA's support for our collaboration work.

REFERENCES

- Unmanned aircraft systems roadmap. Technical report, Office of the Secretary of Defense, 2005.
- IAEA international fact finding expert mission of the nuclear accident following the great east japan earthquake and tsunami. Technical report, International Atomic Energy Agency, 2011. URL <http://www.iaea.org/newscenter/focus/fukushima/missionsummary010611.pdf>.
- Results of airborne monitoring by the ministry of education, culture, sports, science and technology and the U.S. department of energy. Technical report, Ministry of Education, Culture, Sports, Science & Technology in Japan, 2011. URL http://www.mext.go.jp/component/english/_icsFiles/afieldfile/2011/05/10/1304797_0506.pdf.
- J. Ackermann. *Uncertainty and Control*, volume 70 of *Lecture Notes in Control and Information Sciences*, chapter Chapter4: Multi-Model Approaches to Robust Control System Design, pages 108–130. Springer Berlin Heidelberg, Berlin, 1985. doi: 10.1007/BFb0007282.
- T. H. Cox, C. J. Nagy, M. A. Skoog, and I. A. Somers. Civil UAV capability assessment. Technical report, NASA, Dec. 2004.
- Mark Daly, editor. *Jane's Unmanned Aerial Vehicles and Targets*. IHS, Surrey, UK, 2011.
- Y. Miyazawa. Robust flight control system design with multiple model approach. *J. Guidance, Control, and Dynamics*, 15(3):785–788, 1992. doi: 10.2514/3.20908.
- S. Okuyama, T. Torii, A. Suzuki, M. Shibuya, and N. Miyazaki. A remote radiation monitoring system using an autonomous unmanned helicopter for nuclear emergencies. In *Proc. The Fourth Int. Symposium on Radiation Safety and Detection Technology*, pages 414–416, Seoul, Korea, 2008.
- A. Sato and J. Imai. Emergency aerial radiation monitoring system employing unmanned helicopter. Technical Report 47, Yamaha Motor Co., Ltd., November 2011. URL <http://global.yamaha-motor.com/jp/profile/craftsmanship/technical/publish/no47/pdf/gso2.pdf>. (in Japanese).
- M. Sato and K. Muraoka. Flight test verification of flight controller for quad tilt wing unmanned aerial vehicle. In *AIAA Guidance, Navigation, and Control Conference*, Boston, MA, USA, 2013. doi: 10.2514/6.2013-5100. AIAA 2013-5100 (Journal version was accepted).
- K. P. Valavanis, editor. *Advances in Unmanned Aerial Vehicles*, volume 33 of *Intelligent Systems, Control and Automation: Science and Engineering*. Springer, 2007. ISBN 978-1-4020-6114-1.
- K. P. Valavanis, editor. *Recent Developments in Unmanned Aircraft Systems*. Springer, 2012. ISBN 978-94-007-3032-8.
- P. Williams. Three-dimensional aircraft terrain-following via real-time optimal control. *J. of Guidance, Control, and Dynamics*, 30(4):1201–1205, 2007. doi: 10.2514/1.29145.

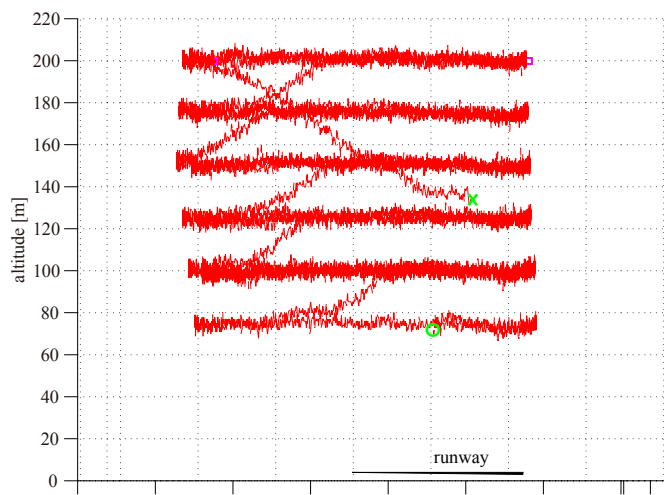


Fig. 8. Vertical view of altitude changes for radiation monitoring demonstration (“x” and “o” respectively denote the autopilot engage and disengage points.)

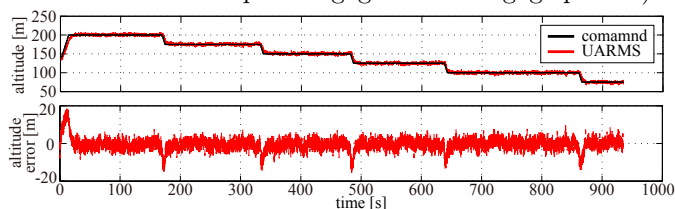


Fig. 9. Time history of altitude and its error

In summary, the altitude errors are almost within 5 [m], and the track course errors on straight lines for the radiation monitoring are almost within 2 [m]. These properties are satisfactory for radiation monitoring. However, as mentioned above, large altitude errors exist when altitude changes are applied, and track course errors due to wind turbulence also exist. Thus, some further revisions are necessary to improve altitude control performance and track course hold control performance.

4. CONCLUSIONS

We address the flight control design for an unmanned airplane for radiation monitoring. The flight control structure is set to be composed of Stability/Control Augmentation System (S/CAS) and guidance loops with Proportional-Integral-Derivative (PID) controllers. The gains in the controllers are designed by optimizing control performance for several models; that is, the worst cost of appropriately defined cost functions among multiple models is minimized to design robust controllers. The designed flight controller was verified to have satisfactory control performance even in windy conditions. Then, demonstration flights were conducted in the near area of Fukushima Dai-ichi nuclear power plant, and it is confirmed that satisfactory control performance was achieved. We use pressure altitude in the demonstration flight; however, GPS altitude signal will be used for the radiation monitoring around the nuclear power plant for precise radiation monitoring. Therefore, the corresponding controller is to be designed. In addition, some further revisions for control logics as well as gains are necessary for further control performance improvement.